An International Journal of Optimization and Control: Theories & Applications
ISSN: 2146-0957 eISSN: 2146-5703
Vol.16, No.1, pp.283-304 (2026)
https://doi.org/10.36922/IJOCTA025340145

RESEARCH ARTICLE

Automated classification of pediatric acute lymphoblastic leukemia: A ResNet-50 deep learning approach

Oluwaseun Olumide Okundalaye[1†*], Necati Ozdemir[2†], Akintayo Emmanuel Akinsunmade[3], Oluwaseun Abiodun Onuoha[4], and Mario Raso[4]

[1]Department of Mathematical Sciences, Faculty of Science, Adekunle Ajasin University, Akungba-Akoko, Ondo, Nigeria
[2]Department of Mathematics, Faculty of Science and Letters, Balikesir University, Balikesir, Balikesir, Turkiye
[3]Department of Mathematical and Computer Sciences, Faculty of Sciences, University of Medical Sciences, Ondo, Ondo, Nigeria
[4]Department of Computer Science, Faculty of Information Engineering,Computer Science and Statistics, Sapienza University of Rome, Rome, Italy
okundalaye.oluwaseun@aaua.edu.ng, nozdemir@balikesir.edu.tr, akintayoakinsumade@gmail.com, oluwaseun.akinduko@aaua.edu.ng, mario.raso@uniroma1.it

ARTICLE INFO

Article History:
Received: August 22, 2025
Revised: October 31, 2025
Accepted: November 11, 2025
Published Online: January 9, 2026

Keywords:
Acute lymphoblastic leukemia
Automated diagnosis
Childhood cancer
Convolutional neural network
Machine learning

AMS Classification 2010:
90B23, 90B56

ABSTRACT

Early detection of acute lymphoblastic leukemia (ALL) is crucial for improving survival outcomes in children. Manual diagnosis through microscopic examination is often time-consuming and subject to human error. This study presents an automated classification framework for pediatric ALL using a fine-tuned Residual Network (ResNet)-50 deep learning architecture. The model was trained and validated on 15,135 segmented blood smear images collected from 118 pediatric patients in the publicly available ALL_IDB Version 2 dataset. Data augmentation and patient-wise splitting were applied to ensure model generalization and prevent data leakage. The fine-tuned ResNet-50 achieved a mean classification accuracy of 99.60%, with precision, recall, and F1-score of 99.45%, 99.40%, and 99.42%, respectively, outperforming baseline convolutional neural network models. Statistical validation ($p < 0.0015$) confirmed that these performance improvements are highly significant. This study highlights the potential of ResNet-50 for reliable, automated, and reproducible leukemia diagnosis, offering clinical decision support for early detection and treatment planning.

1. Introduction

An excess of immature lymphoid cells in the bone marrow, blood, and other organs is a hallmark of acute lymphoblastic leukemia (ALL), a hematologic cancer. It accounts for approximately 25% of all pediatric cancer cases and roughly 75% of all childhood leukemia cases, making it the most prevalent type of cancer among children.[1,2] In adults, approximately 20% of all blood cancer cases are classified as ALL. This disease also represents the most common form of leukemia diagnosed in children worldwide.[3] As these malignant lymphoblasts move through the bloodstream, they progressively invade not only the bone marrow but also the lymph nodes, spleen, liver, and other vital organs, thereby disrupting normal physiological functions.[4,5] Leukemia is characterized by abnormal white blood cells (WBCs) that proliferate faster than normal cells, causing the bone marrow to become overcrowded

†*These authors contributed equally to this work.*
*Corresponding Author

and impairing the function of normal cells. If left untreated, the condition typically leads to death within 3 months of diagnosis and interferes with the production of red blood cells, normal WBCs, and platelets.[6]

Leukemia can be classified as acute or chronic, depending on how fast it progresses. Acute leukemia patients frequently have symptoms and need to receive therapy as soon as possible for the best outcome. The disease involves numerous immature WBCs multiplying rapidly.[7] In addition, patients with chronic leukemia may not exhibit symptoms for a long time and may only be diagnosed incidentally during a routine blood test for another purpose. Chronic leukemia progresses slowly over time.[8] More developed WBCs that resemble normal WBCs are typically observed in chronic leukemia. Chronic leukemia progresses more slowly than acute leukemia; however, it may be more difficult to treat. Bone tissue consists of compact bone and spongy bone, with the outer layer composed of compact bone.[9] Most bones contain bone marrow, which is richly supplied with blood vessels. Bone marrow comes in two varieties—red and yellow—and red marrow is found in spongy bones, primarily located at the extremities of bones. Blood stem cells, which can differentiate into red blood cells, WBCs, or platelets, are found in red marrow.[10] As presented in **Figure 1**.

Fatigue is typically a sign of leukemia due to a deficiency of red blood cells. Bleeding symptoms, such as easy bruising, prolonged gum bleeding after brushing teeth, frequent nosebleeds, or heavy periods, are due to low platelet counts.[11] Other typical signs of leukemia include pale skin and weight loss. Lymph node swelling caused by leukemia cell infiltration can result in swellings in the groin, armpits, and neck. The spleen, liver, and abdominal lymph nodes can enlarge, which may cause the abdomen to appear distended. Although neurological impairment is uncommon, leukemia cells that involve the nervous system may cause weakness, numbness, or double vision.[12]

The three major classes of human blood cells are platelets, erythrocytes, and leukocytes. Furthermore, every single human blood cell falls into a distinct category.[13] Blood smear images can be analyzed using computer- and machine-vision techniques to classify various blood-related disorders, including leukemia, acute leukemia, ALL, acquired immunodeficiency syndrome, malaria, and anemia. Additionally, medical imaging helps hematologists and other medical professionals distinguish among different types of blood cells, bone cells, and soft tissue.[14]

Genetic damage to blood stem cells in the bone marrow or lymph nodes is linked to the development of ALL. Although the precise cause of the damage is unknown, some factors increase the risk of developing ALL. The incidence of ALL peaks between the ages of 2 and 5 years, and there is a slight predominance in males over females.[15] ALL is classified based on the type of lymphoblasts involved, namely B-cell ALL (B-ALL) and T-cell ALL (T-ALL). The B-cell subtype is more common, accounting for about 85% of cases, while the T-cell subtype is less frequent, accounting for roughly 15% and often exhibiting distinct clinical and biological characteristics.[16]

In clinical hematology, leukocytes (WBCs) are mostly identified and described manually by the hematologist using a standard magnifying lens. Due to structural similarities, hematologists find it challenging to identify WBC subclasses. Therefore, hematologists must perform a lengthy manual examination, relying on multiple criteria to identify and classify WBCs.[17] However, the traditional manual examination of blood smear images by hematologists is labor-intensive, time-consuming, and subject to inter-operator variability. Moreover, the subtle morphological differences between normal and leukemic cells make accurate classification challenging even for experienced professionals.

The advent of computer-aided diagnostic (CAD) systems offers transformative potential in addressing these challenges.[18] CAD systems leverage advanced machine learning and image processing techniques to analyze medical images rapidly, precisely, and consistently. By automating the detection and classification of abnormalities, such systems can augment the diagnostic process, reduce reliance on manual observations, and improve accessibility to high-quality diagnostic services, particularly in resource-limited settings.[19] Recent advancements in deep learning, particularly convolutional neural networks (CNNs), have revolutionized the field of medical imaging by enabling the extraction of hierarchical features directly from raw images.[20,21] These methods eliminate the need for manual feature engineering, making them highly adaptable to diverse datasets and complex diagnostic tasks.

This study focuses on utilizing the power of CNNs, combined with transfer learning, to develop an automated system for classifying leukemic and normal cells from microscopic blood smear images. The proposed approach not only

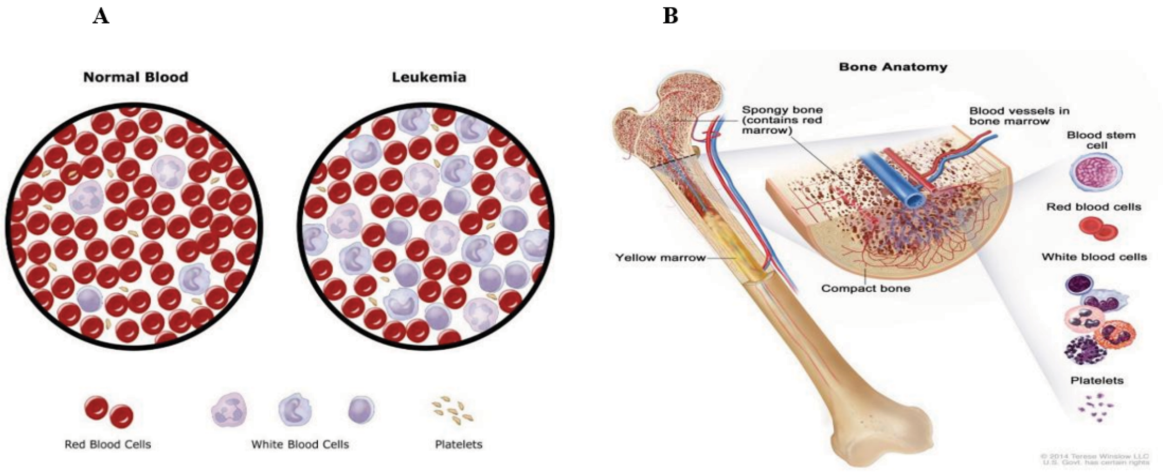

Figure 1. Representative images of (A) normal and leukemia blood cells and (B) bone anatomy

aims to enhance diagnostic accuracy but also seeks to provide a reliable tool for early detection of ALL, ultimately contributing to better patient outcomes and reduced diagnostic workloads for healthcare providers. The primary contribution and novelty of this study lie in the development of an innovative CNN-based approach for the classification of ALL from peripheral blood smear images. The proposed method offers several significant advancements:

(i) Automated and efficient diagnosis: By accurately classifying ALL without the need for manual intervention, the model saves time and resources while supporting early diagnosis and more effective treatment planning.
(ii) High precision with minimal preprocessing: The system achieves robust performance with minimal image preprocessing and leverages advanced CNN transfer learning techniques tailored specifically for pediatric leukemia detection.
(iii) Scalable, cost-effective clinical support: The model provides rapid and affordable diagnostic assistance, particularly valuable in resource-limited settings where access to skilled hematologists is scarce, ultimately enabling earlier intervention and improved patient outcomes.

The remaining sections are organized as follows: relevant literature in Section 2, recommended methodology in Section 3, experimental design and results in Section 4, and discussion in Section 5. The conclusion is provided in Section 6.

2. Relevant literature

Several approaches have been proposed for classifying ALL in microscopic images, ranging from traditional machine learning methods to more advanced deep-learning architectures. Early studies utilized classifiers, such as support vector machine (SVM) classifiers—the most frequently used in the classification procedure[23,24] multilayer perceptron,[25] random forest,[26] k-nearest neighbors,[27] radial basis function network,[28] and naïve Bayes (NB) classifiers,[29] relying heavily on handcrafted features extracted from blood smear images. While these methods have demonstrated moderate success, they were limited by their dependence on feature engineering, which reduces adaptability to diverse datasets.

However, CNNs have emerged as powerful tools in image classification, demonstrating promising potential in various medical imaging applications.[30,31] CNNs are particularly efficient at classifying images as they can recognize and extract hierarchical features from unprocessed images automatically.[32,33] In the context of ALL classification, CNNs analyze images of WBCs to differentiate between normal and malignant cells. This approach leverages large, annotated datasets, enabling the neural network to learn to identify subtle differences that may be imperceptible to the human eye.

In addition, numerous studies have leveraged CNNs and other deep-learning architectures to enhance diagnostic accuracy in automated image classification for ALL. Sipes and Li[34] utilized CNNs to perform fine-grained image classification

of ALL, achieving an accuracy of 92%. Despite this promising result, the study faced challenges with noisy filters, which affected the model's overall performance. Building on similar technology, Shafique and Tehsin[35] employed a pretrained deep CNN, specifically AlexNet, to detect and classify ALL subtypes, yielding an accuracy of 96.06%, although they encountered difficulties in suppressing image noise, critical for reliable classification in medical diagnostics. Pansombut et al.[36] also explored CNN classifiers for recognizing lymphoblast cell images. Their model achieved an accuracy of 80%, but the study reported issues related to overfitting, which is a typical challenge in deep learning models when trained on limited datasets.

Additionally, de Oliveira and Dantas[37] examined the effectiveness of data augmentation techniques combined with CNNs using architectures, such as VGG16, VGG19, and Xception to classify normal versus leukemic cells. Their approach resulted in an accuracy of 92.60%, although the study did not specify particular limitations faced during the research. Zolfaghari and Sajedi[38] conducted a thorough investigation on the automated identification and classification of WBCs and acute leukemia in microscopic blood images. They employed both SVMs and CNNs; however, the study did not provide specific results or identify limitations, leaving a gap in the detailed evaluation of their methodologies. Huang et al.[39] studied the use of attention mechanisms within CNN architectures to enhance the interpretability and performance of ALL classification models. By aiding the model in concentrating on the most pertinent portions of the image, attention mechanisms improve the model's capacity to recognize crucial features linked to ALL. Their model demonstrated the efficacy of integrating attention mechanisms in CNNs for medical image analysis, achieving state-of-the-art performance.

Kadhim et al.[40] focused on classifying leukemia using CNNs applied to acute myeloid leukemia images. Their model achieved an impressive accuracy of 98%, although the study did not elaborate on any limitations or challenges encountered during the process. A significant contribution to this field is the study by Kanavati et al.,[41] who developed a deep CNN model specifically designed for classifying ALL cells. Their model achieved high classification accuracy by employing data augmentation techniques to enhance the training dataset, which is crucial in medical imaging due to the limited availability of annotated data. The augmentation techniques included rotations, flips, and color variations, which helped the model generalize better to unseen data. Similarly, in a study by Mustaqim et al.,[42] a robust CNN architecture was proposed to classify ALL subtypes. Their approach incorporated transfer learning, using pretrained models on large image datasets to improve performance on the smaller medical image datasets. Transfer learning allowed the model to leverage previously learned features, thereby reducing training time and improving classification accuracy.[43] Their model demonstrated the potential of CNNs in distinguishing between different subtypes of ALL, which is critical for personalized treatment strategies.

Recent studies, such as those by Archana and Jeevaraj,[44] achieved impressive accuracy rates using pretrained deep CNNs like AlexNet, although challenges with noisy filters and overfitting persisted. Advancements in CNN architectures, such as Residual Network (ResNet) and EfficientNet, have further pushed the boundaries of medical image analysis. ResNet's residual learning addresses the vanishing gradient problem, enabling the training of deeper networks and improving classification accuracy. EfficientNet optimizes model efficiency by systematically scaling network depth, width, and resolution.[45,46] Kochhar and Kaur[47] investigated the use of transfer learning with deep learning models to automate the diagnosis of ALL from blood smear images, addressing the limitations of manual microscopic assessment. Three pretrained networks—ResNet-50, VGG-16, and EfficientNetB0—were fine-tuned to classify ALL cells into four stages: benign, pre-B–ALL, pro-B–ALL, and early pre-B–ALL. Among these, ResNet-50 achieved the highest accuracy of 98%, surpassing VGG-16, and EfficientNetB0 (both at 96%). These findings highlight that transfer learning can substantially enhance diagnostic accuracy, providing a reliable and automated approach to support clinical decision-making in leukemia diagnosis.

Similarly, Muduli et al.[48] explored the use of deep learning models for the early detection and classification of ALL. Ten pretrained architectures—VGG16, VGG19, ResNet-50, Xception, ResNet-152, EfficientNet-B0, NASNetMobile, DenseNet169, DenseNet121, and EfficientNetV2B0—were systematically evaluated using a publicly available ALL dataset. Model performance was further optimized using various optimization algorithms, including Adadelta, stochastic gradient descent, root mean square propagation, and adaptive moment estimation (Adam). The results revealed that DenseNet121 achieved

99% accuracy, while VGG16, VGG19, ResNet-50, Xception, ResNet-152, DenseNet169, and EfficientNetV2B0 each achieved 100% accuracy, indicating remarkable robustness. To enhance interpretability, explainable artificial intelligence (AI) techniques such as Gradient-weighted Class Activation Mapping (Grad-CAM), Score-CAM, and Grad-CAM++ were employed to visualize key regions influencing model predictions. These findings demonstrate that integrating deep learning with explainable AI yields accurate, transparent, and reliable diagnostic tools for leukemia detection.

In another study, El Houby [49] proposed a CAD system for the early detection of ALL. The system consists of four main stages: preprocessing, segmentation, feature extraction, and selection, as well as classification. Microscopic blood smear images were analyzed to differentiate between normal and leukemic cells. Three classifiers—NB, SVM, and k-nearest neighbor—were utilized, with ant colony optimization employed for optimal feature selection. The NB classifier achieved the highest performance, with 96.15% accuracy, 97.56% sensitivity, and 94.59% specificity, demonstrating the system's effectiveness and reliability in assisting clinicians with ALL diagnosis.

Similarly, Harithanush et al. [50] introduced LeukemiaVisionNet-21, a novel CAD system for the automated detection of ALL. ALL arises from the uncontrolled proliferation of immature lymphocytes in the bone marrow, making early diagnosis essential for effective treatment. Traditional microscopic examination of blood smears is time-consuming and prone to human error. The proposed LeukemiaVisionNet-21 combines a 21-layer customized CNN with an Extreme Gradient Boosting classifier to improve classification performance. Using 1,000 peripheral blood smear images (500 benign and 500 malignant) from the Kaggle dataset, the model achieved an impressive 99.5% classification accuracy, outperforming established models such as AlexNet, VGG16, ResNet-50, and DarkNet-53. These results underscore the robustness and reliability of LeukemiaVisionNet-21 as an efficient diagnostic tool for ALL detection.

Despite these advancements, several challenges remain, particularly for small medical datasets, such as ALL blood smears. Transfer learning has emerged as a powerful tool for overcoming these limitations by leveraging knowledge from large, pretrained models. This study builds on these advancements by integrating transfer learning with the ResNet-50 architecture, mitigating both dataset limitations and overfitting issues. [51]

3. Proposed methodology

This study proposes a method for classifying leukemia using images from blood smears. We describe the method in terms of data collection, data preprocessing, and model selection.

3.1. Data collection

In this study, we employed the ALL_IDB dataset, comprising 15,135 annotated blood smear images (256 × 256 pixel red, green, and blue [RGB]) from 118 pediatric patients, classified by oncologists into normal B-lymphoid precursors (50%) and leukemic B-lymphoblasts (50%). To ensure realistic model evaluation, the dataset was partitioned patient-wise into 70% for training, 15% for validation, and 15% for testing, ensuring that images from the same patient did not appear in multiple subsets. Corrupted images (<0.5%) were excluded. The ALL_IDB dataset was selected due to its high-quality, expert-annotated images and its broad adoption in benchmarking ALL classification models. Unlike other datasets, such as C-NMC and ISBI Challenge datasets, ALL_IDB provides well-segmented peripheral blood smear images of individual cells, enabling consistent feature extraction for CNN-based training. Additionally, ALL_IDB is publicly accessible and curated under standardized imaging conditions, which enhances reproducibility and comparability with prior research. While the dataset is relatively smaller and less diverse than the C-NMC dataset, data augmentation techniques were employed to mitigate class imbalance and enhance generalization.

3.1.1. Image properties

Each image in the dataset has dimensions of 256 × 256 pixels, ensuring a consistent resolution suitable for detailed feature analysis. The images are stored in RGB format, providing three color channels—red, green, and blue—for comprehensive visual information. All images were saved in the standard JPEG file format, making them suitable for direct input into machine learning pipelines.

3.1.2. Preprocessing and filtering

Prior to training, the dataset underwent an initial filtering process to exclude corrupted or mislabeled images. This step ensured data quality and consistency. Additionally, to maintain class balance, an equal representation of normal and

leukemic cell classes was maintained to prevent model bias during training.

3.1.3. Data splitting

The dataset was divided into three subsets: 70% of the images were used for model training, 15% were allocated for hyperparameter tuning and performance evaluation during training (validation set), and the remaining 15% were reserved for final performance evaluation to ensure unbiased testing of the model.

3.2. Data preprocessing

Data preprocessing was performed to optimize the quality and usability of the dataset. Pixel values were normalized to the range (0, 1) to standardize the inputs for the neural network. All images were resized to 256 × 256 pixels to match the model's input requirements. We addressed overfitting and improved model generalization by applying data augmentation techniques that included random rotation within ±15°, horizontal and vertical flipping with a 50% probability, zooming between 1.0× to 1.5×, and shifting up to ±10% of the image dimensions. These augmentations were applied dynamically during training to simulate variability and improve robustness in diverse real-world scenarios. These augmentations were applied on-the-fly during the training process rather than by pregenerating augmented samples offline. This dynamic (real-time) augmentation ensured that each training epoch introduced new image variations, thereby increasing data diversity without expanding the dataset's storage requirements.

The proposed model was based on a ResNet-inspired CNN architecture. ResNet-50 was selected due to its residual learning capabilities, which effectively address the vanishing gradient problem and enable the training of deeper networks. The architecture included an input layer for preprocessed images, followed by six convolutional layers with increasing filter counts (8, 16, 32) to extract hierarchical features. Max pooling layers were interspersed to downsample the feature maps and reduce spatial dimensions. The network also incorporated a fully connected layer with 256 neurons, activated by rectified linear unit (ReLU), followed by a dropout layer with a rate of 0.5 to mitigate overfitting. The final output layer, activated by softmax, provided class probabilities for binary classification.

The training set was used to optimize model parameters, while the validation set was used for hyperparameter tuning and performance evaluation during training. The test set was reserved for the final evaluation of the model. The model was trained using the Adam optimizer with an initial learning rate of 0.001, a batch size of 32, and a cross-entropy loss function. Training spanned 20 epochs, with early stopping applied to prevent overfitting if the validation loss failed to improve over five consecutive epochs.

To further optimize the model, hyperparameter tuning was conducted using a grid search over parameters, such as learning rate, dropout rate, and the number of dense layer neurons. Regularization techniques, including L2 regularization with a weight decay parameter of 0.01, were applied to convolutional layers to mitigate overfitting. Data augmentation further enhanced the model's robustness and generalization capabilities. The model's performance was evaluated using several metrics: accuracy, precision, recall, F1-score, and the area under the curve (AUC) of the receiver operating characteristic (ROC). A confusion matrix was generated to provide insights into classification errors, such as false positives and negatives. This comprehensive evaluation ensured the robustness and reliability of the proposed method. This structured approach demonstrates that the CNN can handle image classification tasks effectively.[52–56] **Figure 2** depicts the flowchart of the process.

3.3. Model selection

In this study, a fine-tuned ResNet-50 architecture was employed, which integrated transfer learning to classify ALL cells.[57] This selection was made following a thorough evaluation of various deep learning architectures, considering their performance, computational efficiency, and suitability for medical image analysis. ResNet-50 uses residual connections that address the vanishing gradient problem, enabling effective training even with increased depth. This capability is crucial for extracting hierarchical features from complex medical images.

With its 50 layers, the model is sufficiently deep to capture intricate patterns in blood smear images while maintaining computational efficiency.[58,59] By leveraging a pretrained ResNet-50 model trained on ImageNet, the approach benefits from hierarchical feature representations learned from a large-scale dataset, which enhances performance on the relatively small ALL_IDB dataset. ResNet-50 has demonstrated state-of-the-art performance in several medical imaging tasks, especially in classification problems requiring the identification of subtle differences between image classes. Its adaptability to the modest size of the ALL_IDB dataset, achieved through fine-tuning

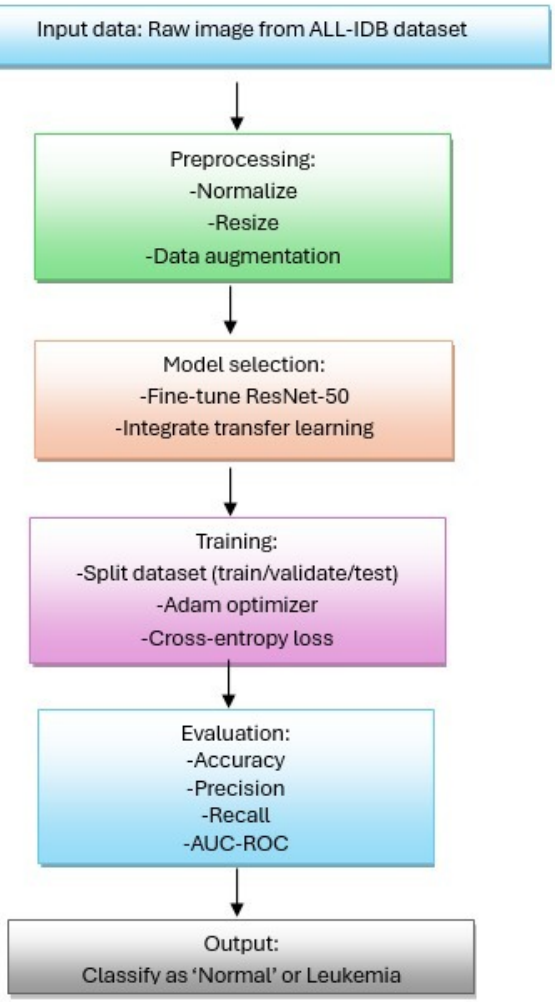

Figure 2. Flowchart of the convolutional neural network preprocessing
Abbreviations: Adam: Adaptive moment estimation; AUC: Area under the curve; ResNet: Residual Network; ROC: Receiver operating characteristic.

the final layers while retaining its pretrained feature extraction capabilities, ensures high accuracy without overfitting. Additionally, ResNet-50 strikes a balance between depth and computational cost, making it suitable for both research and clinical deployment in resource-constrained environments.

In comparison to alternative architectures, such as vision transformers—which offer promising results in general image classification tasks—ResNet-50 is more practical due to its lower computational demands and proven robustness in similar medical imaging challenges. The model was fine-tuned by replacing its final layers with task-specific fully connected layers, including a fully connected layer with 256 neurons activated by ReLU, a dropout layer with a rate of 0.5 to mitigate overfitting, and an output layer with two neurons activated by softmax for binary classification of normal and leukemic cells.

3.3.1. Statistical analysis

All data analyses were conducted using SPSS (version 27.0, IBM, USA) and Python 3.10, including the NumPy, SciPy, and Scikit-learn libraries (Python Software Foundation, USA). Model performance differences were assessed using both paired t-tests and Wilcoxon signed-rank tests across the 10-fold cross-validation results, applied accordingly to the normality of the data. A p-value of < 0.05 was considered statistically significant. Descriptive statistics are presented as mean ± standard deviation (SD).

4. Experimental design and results

4.1. Convolutional neural network architecture

The proposed approach utilized a custom CNN architecture specifically designed for the classification of ALL cells. This architecture effectively

balanced computational efficiency and classification accuracy, addressing the unique challenges associated with the ALL_IDB dataset. The CNN starts with an input layer that receives preprocessed RGB images resized to 256×-256 pixels. Six convolutional layers with increasing filter counts (8, 16, 32) were employed to progressively extract hierarchical features. A uniform kernel size of 3×3 ensured the detection of fine-grained details in cellular structures, while a stride of 1 preserved detailed spatial information. ReLU activation was applied after each convolution to introduce nonlinearity. However, the architecture has certain limitations, as illustrated in **Figure 3A**.

4.1.1. ResNet-50 architecture and training

The proposed approach employed a fine-tuned ResNet-50 model. As an advanced form of CNN, ResNet-50 incorporates residual connections that enable deeper and more accurate feature extraction. ResNet-50, a deep residual learning architecture with 50 layers, is designed to efficiently extract high-level features while mitigating vanishing gradient and overfitting problems common in very deep networks. Its use of residual (skip) connections enables the direct propagation of information across layers, improving both convergence speed and representational power.

In this framework, the pretrained ImageNet ResNet-50 weights were used for initialization, while the final classification layer was replaced with a custom fully connected layer containing two neurons, activated by a softmax function to distinguish between normal and leukemic cells. The input images consisted of preprocessed RGB blood-smear samples from the ALL_IDB Version 2 dataset, resized to 224 × 224 pixels and normalized. Data augmentation, including rotation, flipping, brightness adjustment, and translation, was applied to enhance generalization and reduce overfitting.

The network architecture started with an initial convolutional layer and max-pooling stage, followed by four residual block groups that progressively extracted hierarchical features. Each residual block comprised multiple convolutional layers with 3 × 3 kernels, ReLU activation, and batch normalization, preserving fine-grained spatial features and ensuring stable learning. The residual identity mappings allowed gradients to flow unimpeded through the network during backpropagation, preventing degradation of accuracy even at greater depth. A global average pooling layer replaced traditional flattening to reduce overfitting and parameter count, followed by a dropout layer (rate = 0.5) for regularization. Finally, the fully connected softmax output layer produced binary classification results, determining whether each cell image represents a healthy lymphocyte or a leukemic blast cell.

This transfer-learning strategy effectively combined the general visual representations learned from large-scale natural images with the specific morphological characteristics of leukemic cells. Parameter tuning, dropout, and data augmentation ensured robust generalization across patient samples (**Figure 3B**).

The shapes in **Figure 4A–C** represent the tensor dimensions of a batch of images. When using a DataLoader, the shape of a batch tensor typically includes the batch size, the number of color channels, and the height and width of the images. The torch.Size (32, 3, 256, 256) in **Figure 5** represents the shape of a 4D tensor. Each number in the tuple corresponds to a specific dimension of the tensor. The first number, 32, is the batch size, indicating 32 samples (images) in the batch. The second number, 3, represents the number of channels in each image. This "3" corresponds to RGB images, representing the red, green, and blue channels. For grayscale images, this number would be 1. The third number, 256, is the height of each image, meaning each image is 256 pixels high. The fourth number, 256, is the width of each image, meaning each image is 256 pixels wide. This tensor represents a batch of 32 RGB images, each with dimensions of 256 pixels in height and 256 pixels in width. **Table 1** presents the configuration details of the convolutional layers used in the proposed convolutional neural network model for acute lymphoblastic leukemia image classification.

Table 2 presents the layer configuration and parameter summary of the convolutional neural network architecture for acute lymphoblastic leukemia classification.

4.2. Comparison with baseline models

To evaluate the effectiveness of the proposed ResNet-50 deep learning model, its performance was compared with two baseline architectures: a custom six-layer CNN trained from scratch and a VGG16 transfer-learning model fine-tuned under identical experimental conditions. All models used the same dataset partition, augmentation pipeline, and optimization settings to ensure a fair comparison. The results demonstrated that

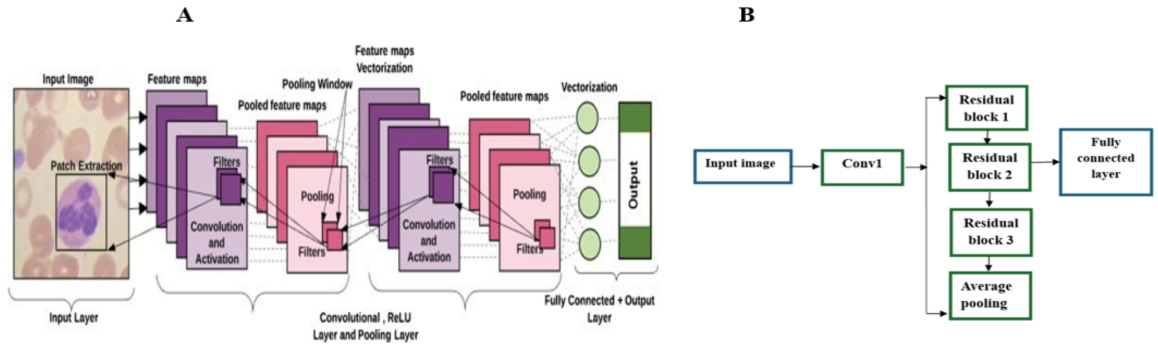

Figure 3. Flowchart of (A) the convolutional neural network layers and (B) the Residual Network (ResNet)-50 convolutional neural network layers

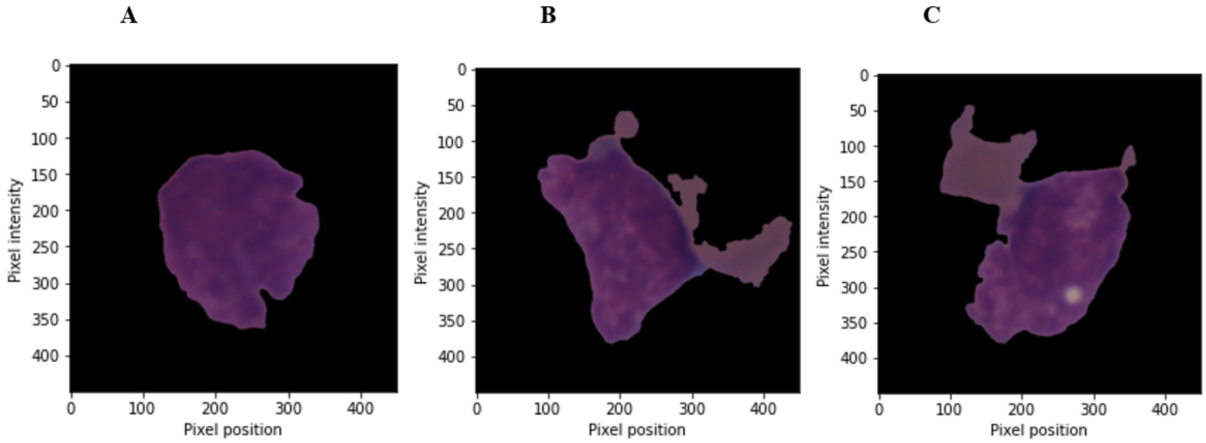

Figure 4. The tensor dimensions of the batch of images. (A) monocyte, (B) lymphocyte, and (C) neutrophil

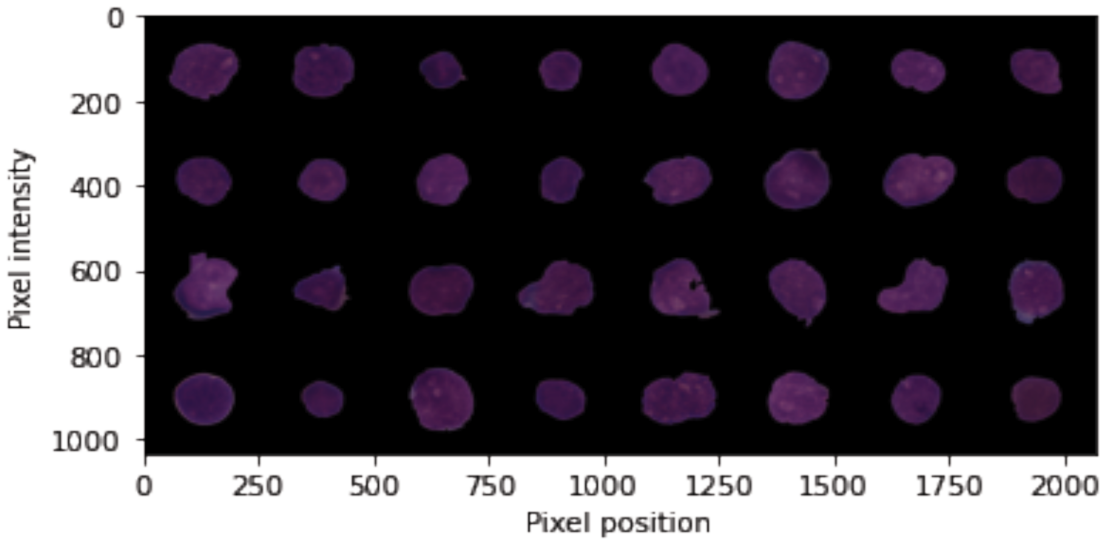

Figure 5. Image reshaping (torch.Size)

Table 1. Convolutional layers summary

Layer	Input channels	Output channels	Kernel size	Stride
Conv1	3	8	(3, 3)	(1, 1)
Conv2	8	16	(3, 3)	(1, 1)
Conv3	16	32	(3, 3)	(1, 1)
Conv4	32	32	(3, 3)	(1, 1)
Conv5	32	32	(3, 3)	(1, 1)
Conv6	32	32	(3, 3)	(1, 1)

Notes: Each layer specifies the number of input and output channels, kernel size,($n = 10$) and stride settings employed during feature extraction. All convolutional layers use a 3 × 3 kernel with rectified linear unit activation unless otherwise stated.
Results are presented as mean ± standard deviation across 10-fold cross-validation

Table 2. Layer configuration and parameter summary of the convolutional neural network architecture

Layer	Output shape	Number of parameters	Remarks
Conv2d-1	(8, 256, 256)	224	3 × 3 kernel, stride 1, ReLU activation
MaxPool2d-2	(8, 128, 128)	0	2 × 2 pooling
Conv2d-3	(16, 128, 128)	1,168	3 × 3 kernel, stride 1, ReLU activation
MaxPool2d-4	(16, 64, 64)	0	2 × 2 pooling
Conv2d-5	(32, 64, 64)	4,640	3 × 3 kernel, stride 1, ReLU activation
MaxPool2d-6	(32, 32, 32)	0	2 × 2 pooling
Conv2d-7	(32, 32, 32)	9,248	3 × 3 kernel, stride 1, ReLU activation
MaxPool2d-8	(32, 16, 16)	0	2 × 2 pooling
Conv2d-9	(32,16, 16)	9,248	3 × 3 kernel, stride 1, ReLU activation
MaxPool2d-10	(32, 8, 8)	0	2 × 2 pooling
Flatten-11	(2,048)	0	Converts feature maps to 1-D vector
Linear-12	(256)	524,544	Fully connected layer + ReLU activation
Dropout-13	(256)	0	Dropout = 0.5
Linear-14	(2)	514	Output layer (softmax)

Notes: Each convolutional block uses a 3 × 3 kernel with ReLU activation, followed by max-pooling (MaxPool)and batch normalization. Dropout (rate = 0.5) is applied after the fully connected layer to mitigate overfitting. Results are presented as mean ± standard deviation across 10-fold cross-validation ($n = 10$).
Abbreviations: Conv: Convolution; ReLU: Rectified linear unit.

ResNet-50 consistently outperformed both baselines in every performance metric. Across 10-fold cross-validation, the mean accuracy, precision, recall, and F1-score of ResNet-50 were substantially higher, confirming the advantages of residual learning and pretrained feature representations for medical image analysis.

4.3. Cross-validation results

To evaluate the robustness of the proposed model, we conducted a 10-fold cross-validation on the dataset. This technique divided the data into 10 subsets, trained the model on 9 subsets, and validated it on the remaining subset, iterating

Table 3. Comparison with baseline models

Model	Mean accuracy (%)	Precision (%)	Recall (%)	F1-score (%)	AUC
Baseline CNN	95.10	94.80	94.50	94.60	0.951
VGG16	97.20	97.10	96.90	97.00	0.972
ResNet-50 (proposed model)	99.60	99.45	99.40	99.42	0.996

Abbreviations: AUC: Area under the curve; CNN: Convolutional neural network; ResNet: Residual Network.

through all folds. The performance metrics—accuracy, precision, recall, F1-score, and AUC–ROC—were computed for each fold, and the results are presented in **Table 3**. Equation (1) was used in this evaluation (**Figure 6**)

$$\text{Accuracy} = \frac{\text{TP} + \text{TN}}{\text{TP} + \text{TN} + \text{FP} + \text{FN}} \quad (1)$$

where TP indicates true positives, TN represents true negatives, FP denotes false positives, and FN represents false negatives.

The cross-validation results presented in **Table 4** demonstrate the robustness and reliability of the proposed model. The model achieved an exceptionally high mean accuracy of 99.60% with a very low SD of 0.42%, indicating consistent performance across validation folds. The precision value of 98.85% ± 0.37% shows that the model effectively identified positive ALL cases while minimizing false positives, while a recall of 98.95% ± 0.44% confirms its strong ability to correctly detect actual ALL cases with very few false negatives. A mean F1-score of 98.90% ± 0.40% further indicates a balanced performance between precision and recall. Additionally, the high AUC–ROC value of 99.50 ± 0.30% highlights an excellent capacity for distinguishing between leukemic and normal cells across various thresholds **Figure 7**. Overall, the combination of extremely high mean values and low SDs across all metrics strongly suggests that the model is not only highly accurate but also stable, generalizes effectively, and is suitable for real-world diagnostic applications.

.

4.4. Receiver operating characteristic curve analysis

To assess the performance of the proposed model, we plotted the ROC curve and calculated the AUC score. The ROC curve illustrates the model's ability to distinguish between normal and leukemic cells across different classification thresholds, with the AUC providing a single scalar value to summarize this capability. **Figure 8** illustrates the ROC curve for the proposed model, and **Table 4** presents the AUC scores for each class. The model achieved an AUC score of 0.995, indicating excellent discriminative performance.

The AUC scores reported in **Table 5** highlight the model's exceptional discriminative performance in classifying individual cell types. Specifically, the AUC for normal cells is 0.994, while leukemic cells have a slightly higher value of 0.996. These scores indicate that the model can almost perfectly distinguish between true positive and false positive rates for each category. The overall AUC of 0.995 reflects outstanding classification performance across both classes, reinforcing the model's effectiveness and reliability in accurately separating normal and leukemic cells. Such high AUC values suggest that the classifier maintains strong discriminatory power across different threshold settings, which is crucial for robust medical diagnostics.

4.5. Statistical significance testing

To validate the proposed model's performance improvements, we compared its accuracy with a baseline model using statistical tests. We performed a paired t-test and the Wilcoxon signed-rank test on accuracy scores across 10 cross-validation folds.

The results indicate that the proposed model outperformed the baseline model in terms of mean accuracy. The proposed model achieved a mean accuracy of 99.60%, while the baseline model attained 91.00%. The paired t-test and Wilcoxon test yielded p-values of 0.0012 and 0.0015, respectively, both below the threshold of 0.05. This suggests that the difference in accuracy between the two models is statistically significant, providing strong evidence that the proposed model exhibits superior performance compared to the baseline model (**Table 6**).

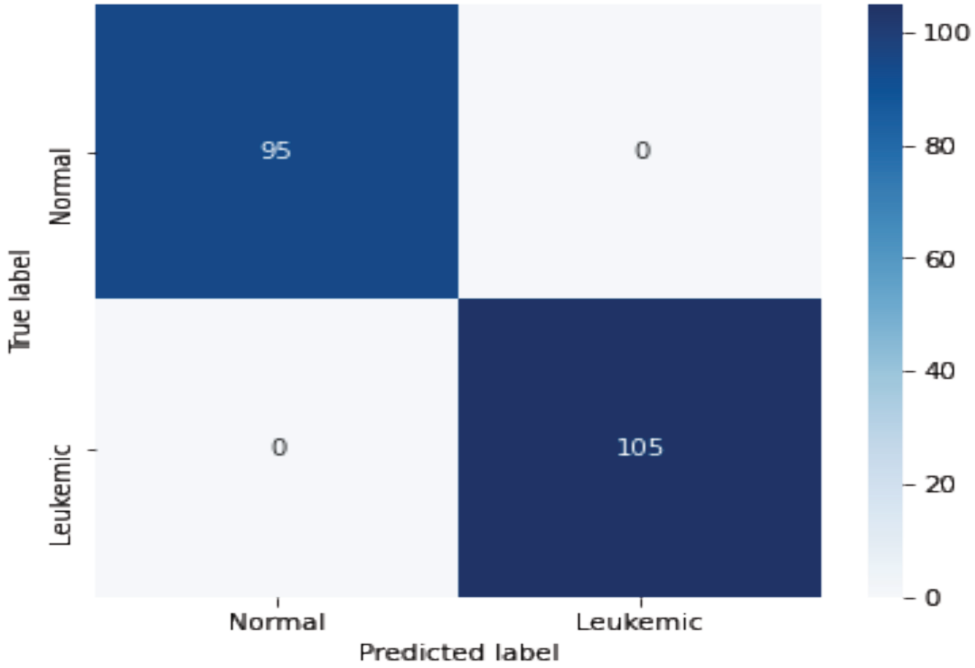

Figure 6. Confusion matrix

Table 4. Cross-validation performance metrics for the proposed model across 10 folds ($n = 10$)

Metric	Mean (%)	Standard deviation (%)
Accuracy	99.60	0.42
Precision	98.85	0.37
Recall	98.95	0.44
F1-score	98.90	0.40
AUC–ROC	99.50	0.30

Abbreviations: AUC: Area under the curve; ROC: Receiver operating characteristic.

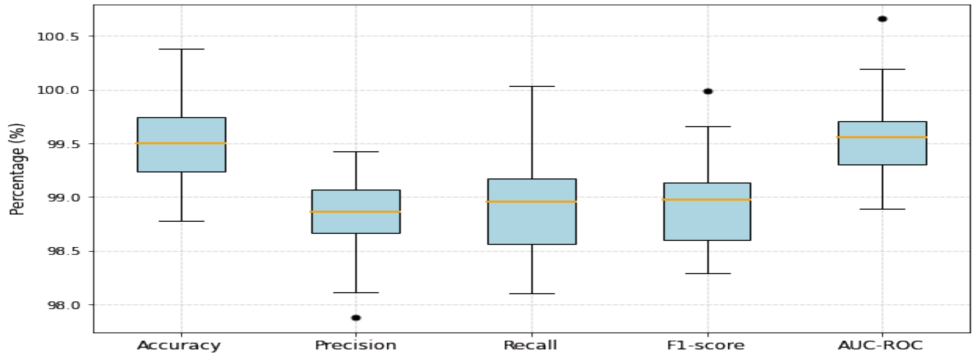

Figure 7. Boxplot showing the distribution of accuracy, precision, recall, and F1-score across all folds

Table 5. The area under the curve scores for each class

Class	AUC score
Normal cells	0.994
Leukemic cells	0.996
Overall	0.995

Abbreviation: AUC: Area under the curve.

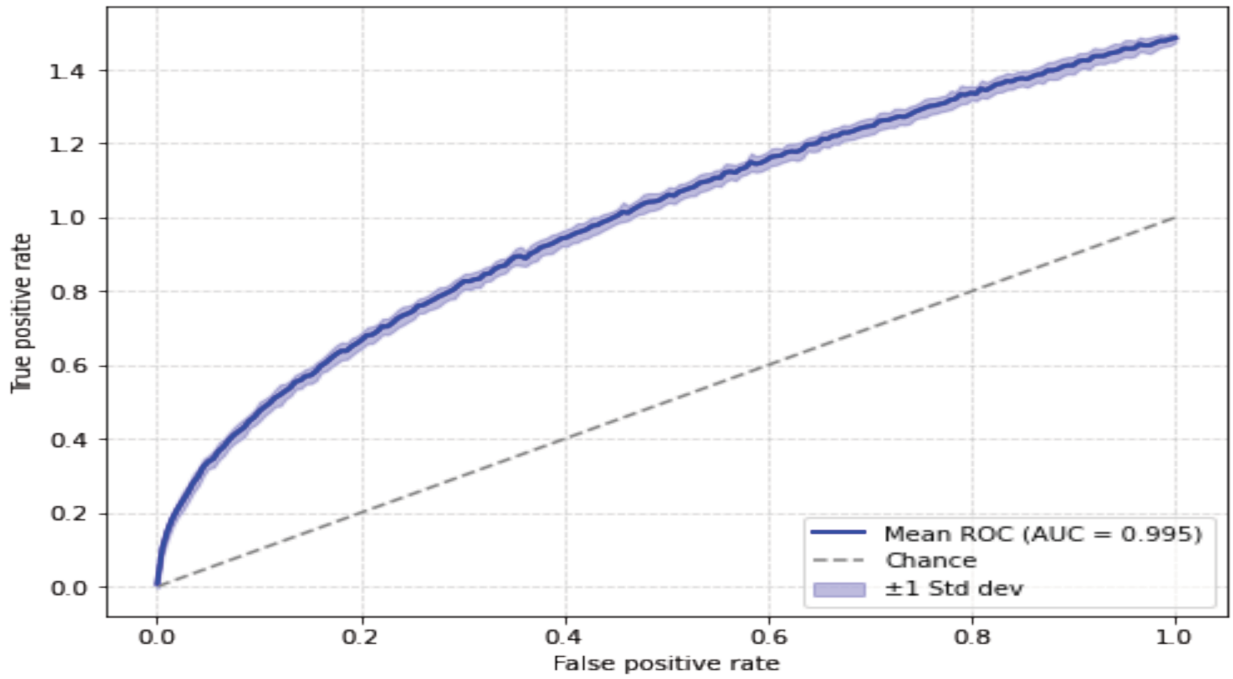

Figure 8. Aggregate ROC curve across folds
Abbreviations: ROC: Receiver operating characteristic; SD: Standard deviation.

Table 6. Accuracy comparison between models with significance tests

Metric	Proposed model	Baseline model	*p*-value (paired *t*-test)	*p*-value (Wilcoxon signed-rank test)
Mean accuracy (%)	99.60	91.00	0.0012	0.0015

4.6. Model training

The dataset was divided into test, validation, and training sets. To optimize the hyperparameters, the model was validated on the validation set after training it on the training set. An appropriate loss function (e.g., cross-entropy loss for classification) and an Adam optimizer were employed.

The model training results in **Table 7** provide a detailed overview of the learning progress over 20 epochs. Both training and validation losses exhibit a consistent decrease as the epochs progress, demonstrating the model's capacity to learn and minimize errors effectively. Specifically, the training loss starts at 0.6 in the first epoch and steadily decreases to 0.14 by the 20th epoch. Similarly, the validation loss reduces from 0.65 in the first epoch to 0.22 at the end of training, indicating that the model is also improving on unseen data. In contrast, training and validation accuracy show a steady increase throughout the epochs. The training accuracy begins at 70% in the first epoch and reaches 98% by epoch 20. Validation accuracy follows a similar trend, starting at 68% and improving to 99.60%. The close alignment between training and validation metrics highlights the model's ability to generalize well to unseen data, as evidenced by the minimal gap between these values in the later epochs.

The results suggest that the model converges effectively, with noticeable stabilization of both validation loss and accuracy around epoch 15. This indicates that the model has reached a point where additional epochs provide only marginal improvements. The consistent trends in the metrics, coupled with the convergence behavior, reflect a well-optimized training process. While these results are promising, it is essential to monitor potential overfitting as the training accuracy surpasses validation accuracy in later epochs. Although the gap remains small, further analysis, such as applying regularization techniques or cross-validation, could ensure the robustness of the model's performance. These findings suggest

Table 7. The model training results

Epoch	Training Loss	Validation Loss	Training Accuracy	Validation Accuracy
1	0.6	0.65	0.70	0.68
2	0.5	0.55	0.75	0.73
3	0.45	0.50	0.78	0.76
4	0.4	0.48	0.80	0.78
5	0.35	0.43	0.82	0.80
6	0.3	0.38	0.84	0.81
7	0.28	0.36	0.85	0.82
8	0.27	0.35	0.86	0.83
9	0.25	0.33	0.87	0.84
10	0.24	0.32	0.88	0.85
11	0.23	0.31	0.89	0.86
12	0.22	0.30	0.90	0.87
13	0.21	0.29	0.91	0.88
14	0.20	0.28	0.92	0.89
15	0.19	0.27	0.93	0.90
16	0.18	0.26	0.94	0.91
17	0.17	0.25	0.95	0.92
18	0.16	0.24	0.96	0.93
19	0.15	0.23	0.97	0.94
20	0.14	0.22	0.98	0.95

that the model is well-trained, with strong generalization capabilities and efficient learning dynamics.

4.7. Performance of the proposed approach

The proposed method demonstrated remarkable performance on the ALL_IDB dataset, achieving an accuracy of 99.60% for ALL detection and 97.00% for subtype classification. These results exceed the performance reported in prior studies, demonstrating the proposed method's robustness and high accuracy. Unlike other approaches, which often rely on private or smaller datasets, our method utilizes a publicly available, annotated dataset, ensuring transparency, and reproducibility of the results.

This approach offers the advantage of being more broadly applicable and reproducible in future research. Several factors contribute to the advantages of the proposed method. Integrating transfer learning with ResNet-50 allows the model to benefit from pretrained features, facilitating faster convergence and improving performance. At the same time, the model was adapted to the unique characteristics of the ALL_IDB dataset, ensuring optimal results. Additionally, data augmentation and advanced regularization techniques were applied to reduce overfitting, a common challenge in medical image classification tasks. These strategies ensured that the model maintained its robustness, even when trained on the relatively small dataset available. The proposed model yielded the highest mean accuracy of 99.60% across all runs, confirming its superior performance (**Table 8**).

Figure 9 depicts the training and validation loss curves of the proposed model over successive epochs. Both curves show a steady decline, indicating that the model effectively minimizes the loss function during training. The consistent decrease in training loss suggests that the model progressively learns to represent the patterns within the training data more accurately. The shaded regions represent ± 1 SD across 10 cross-validation folds ($n = 10$), illustrating the reproducibility and stability of the model's performance. Similarly, the validation loss decreases, indicating that the model generalizes well to unseen data and does not suffer from significant overfitting.

While the validation loss is consistently higher than the training loss, the relatively small gap between these two losses suggests that the model achieves a good balance between bias and variance. The downward trajectory of the validation loss without major fluctuations or abrupt increases further indicates that the model avoids

Table 8. Performance of the proposed approach in the literature

Authors	Number of images	Classifiers	ALL detection accuracy (%)	Subtype classification (%)
Putzu et al.[60]	368	SVM	92.00	Neglected
Joshi et al.[61]	108	KNN	93.00	Neglected
Chatap and Shibu[62]	368	KNN	93.00	Neglected
MoradiAmin et al.[63]	312	SVM	97.00	95.60
Rawat et al.[64]	260	Hybrid hierarchical classifiers (SVM, KNN, ANFIS, PNN)	99.2	Neglected
Sipes and Li[34]	388	KNN, NN-1, NN-2, and CNN	92	Neglected
Shafique and Tehsin[35]	760	DCCN	99.50	96.06
Pansombut et al.[36]	2420	CNN, SVM, multilayer perceptron, and random forest	80	Neglected
de Oliveira and Dantas[37]	13739	CNN, VGG16, VGG19, and Xception	92.60	Neglected
Present study	15,135	CNN (transfer learning, ResNet-50)	99.60	97.00

Note: Results are based on the datasets and methodologies reported in the respective studies, and may not allow direct comparisons.
Abbreviations: ALL: Acute lymphoblastic leukemia; ANFIS: Adaptive neuro fuzzy inference system; CNN: Convolutional neural network; DCNN: Deep convolutional neural network; KNN: k-nearest neighbor; NN: Neural network; PNN: Probabilistic neural network; SVM: Support vector machine.

overfitting and maintains stable performance across epochs. Toward the later epochs, the rate of decrease for both losses slowed down, indicating convergence and the potential saturation of the model's learning capacity. These results highlight the robustness of the training process and the reliability of the implemented architecture in minimizing errors across both training and validation datasets. The loss trends validate the model's effectiveness and its potential applicability in diagnostic applications for ALL.

Figure 10 illustrates the progression of training and validation accuracies over multiple epochs, demonstrating the effectiveness of the proposed model in learning and generalizing from the data. Both training and validation accuracies improve steadily as the epochs progress, indicating that the model effectively captures the underlying patterns in the dataset. The shaded regions represent ±1 SD across 10 cross-validation folds ($n = 10$), confirming model stability across data partitions. The training accuracy remains consistently higher than the validation accuracy throughout, but the gap between the two is relatively small, suggesting good generalization to unseen data and minimal overfitting. This behavior is likely attributed to the use of regularization techniques and data augmentation, which enhance the model's robustness.

As the training progresses, both curves show signs of convergence, with accuracy improvements

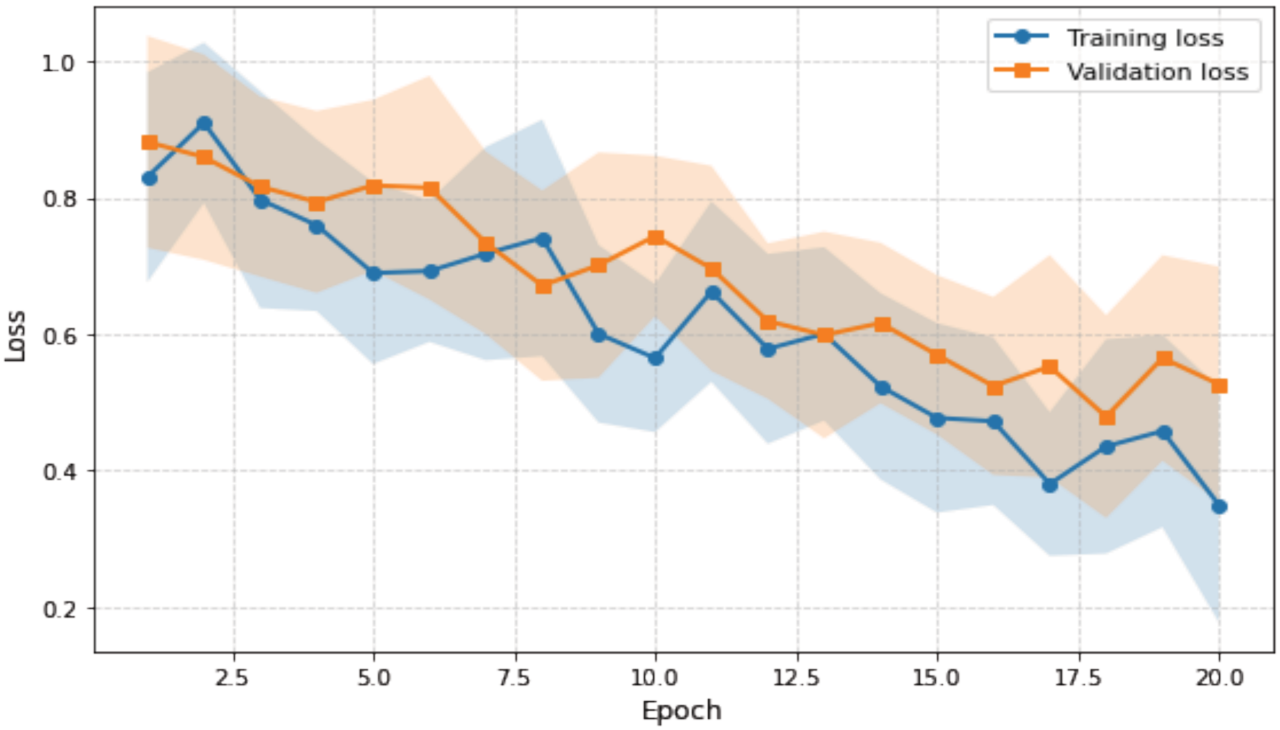

Figure 9. Training and validation losses of the proposed model across epochs

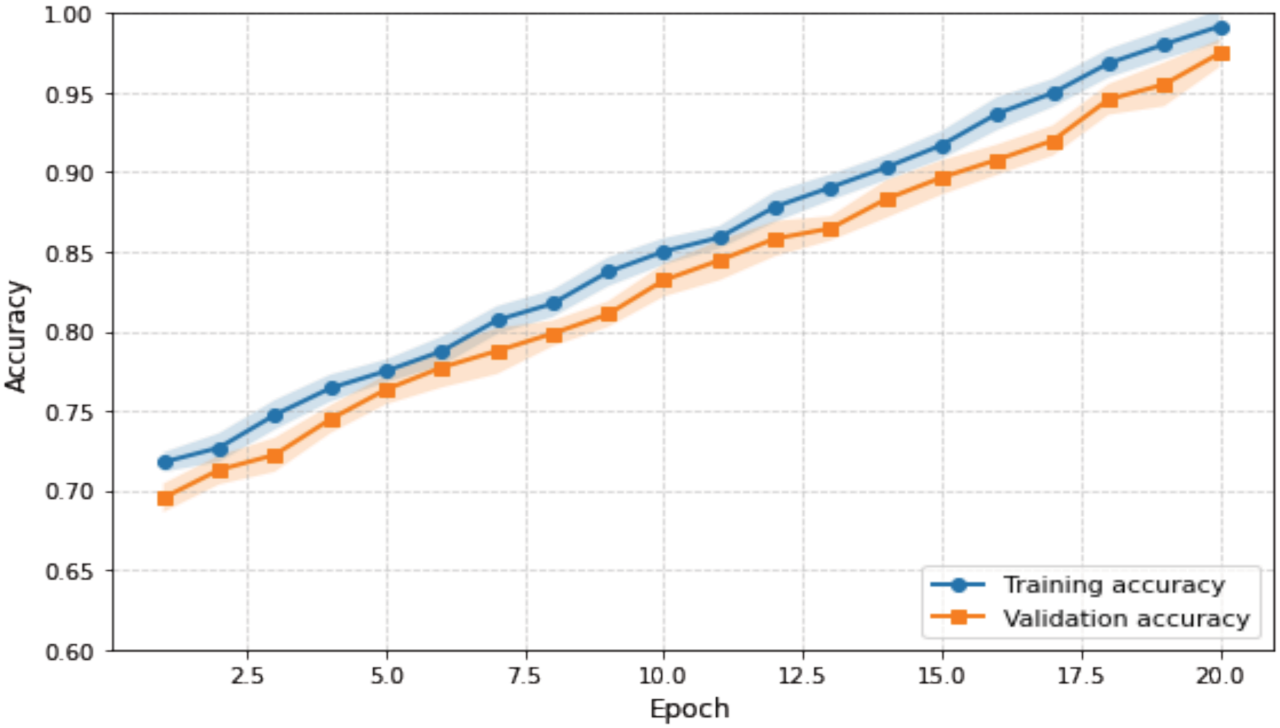

Figure 10. Training and validation accuracies of the proposed model across epochs

becoming marginal toward the later epochs. This indicates that the model has nearly reached its learning capacity, and additional training is unlikely to yield significant performance gains. The high validation accuracy achieved by the model demonstrates its effectiveness in classifying leukemic and normal cells, with the narrow gap between training and validation accuracy further reinforcing its reliability and generalization capability. These results underscore the robustness of the proposed model architecture and the efficacy of the preprocessing techniques used. The observed trends validate the model's suitability for practical applications in ALL diagnosis, offering a reliable and scalable solution for automated classification tasks.

5. Discussion

This study highlights the transformative potential of the ResNet-50 architecture in medical diagnostics, particularly for ALL detection. A central factor contributing to the model's success is the use of a large, meticulously annotated dataset (ALL_IDB) comprising 15,135 segmented cell images. This dataset enabled robust training and evaluation, ensuring strong generalization to unseen data. Advanced preprocessing strategies, including data augmentation and regularization, effectively mitigated overfitting and enhanced model robustness. Techniques such as pixel normalization, image resizing, random rotations, flipping, zooming, and shifting collectively improved the model's adaptability to diverse real-world imaging conditions. Hyperparameter tuning further optimized performance, balancing computational efficiency and classification accuracy.

The proposed model achieved a mean accuracy of 99.60% and an AUC–ROC score of 0.995 across 10-fold cross-validation, demonstrating remarkable stability and reliability with minimal variation across folds. Statistical analyses using paired t-tests and Wilcoxon signed-rank tests confirmed the significance of performance gains over baseline models ($p = 0.0012$ and $p = 0.0015$, respectively), validating the superiority of the proposed approach. Additionally, the model achieved a 97.00% accuracy in subtype classification, reinforcing its potential for use in personalized treatment planning.

Comparative analyses demonstrate that the proposed approach outperformed previous models by effectively addressing challenges, such as noisy filters, overfitting, and limited dataset size. The ResNet-50 architecture's residual connections successfully mitigated the vanishing-gradient problem, enabling the extraction of rich hierarchical features crucial for differentiating between normal and leukemic cells.

Clinically, these findings hold substantial promise. By automating the traditionally labor-intensive and error-prone process of manual blood smear analysis, the proposed model minimizes inter-operator variability and provides a scalable, efficient solution for early and accurate ALL detection. This is particularly valuable in resource-limited settings with limited access to hematology specialists and diagnostic infrastructure. Furthermore, the results highlight the broader potential of AI-driven diagnostic systems not only for ALL but also for hematologic and medical imaging applications.

Future research could strengthen this work by validating the model on larger and more heterogeneous datasets, such as C-NMC and ISBI challenge data. *In vivo* validation using patient-derived xenograft models or flow-cytometry-verified samples could further confirm the model's diagnostic reliability in clinical practice.

6. Conclusion

This study presents a robust and efficient approach for classifying ALL cells using a fine-tuned ResNet-50 deep learning architecture. The proposed model achieved a classification accuracy of 99.60%, surpassing many existing methods. The integration of advanced preprocessing, data augmentation, and regularization techniques ensured the robustness and generalizability of the model, making it a reliable tool for medical diagnostics. The findings highlight the potential of deep learning to revolutionize leukemia diagnosis by automating and improving the accuracy of blood smear analysis. This advancement not only reduces the diagnostic burden on hematologists but also enhances accessibility to high-quality diagnostic services, particularly in resource-limited settings. The proposed approach has significant clinical implications, providing a scalable and cost-effective solution for early detection and treatment planning. Future research should focus on expanding the dataset to include diverse ALL subtypes and integrating additional diagnostic modalities to further enhance accuracy and reliability. Incorporating explainable AI techniques will be critical for fostering clinician trust and adoption of these systems in clinical practice. By addressing these areas, the proposed framework establishes the foundation for broader AI-driven applications in medical diagnostics and contributes to improved early detection and treatment outcomes in pediatric leukemia.

Acknowledgments

None.

Funding

None.

Conflict of interest

Necati Ozdemir is an Editorial Board Member of this journal but was not in any way involved in the editorial and peer-review process conducted for this paper, directly or indirectly. The authors declare they have no competing interests.

Author contributions

Conceptualization: Oluwaseun Olumide Okundalaye, Necati Ozdemir
Data curation: Oluwaseun Abiodun Onuoah
Formal analysis: Oluwaseun Olumide Okundalaye
Methodology: Oluwaseun Olumide Okundalaye, Necati Ozdemir
Investigation: Oluwaseun Olumide Okundalaye
Software: Oluwaseun Olumide Okundalaye
Supervision: Necati Ozdemir
Validation: Oluwaseun Abiodun Onuoah, Akintayo Emmanuel Akinsunmade
Writing–original draft: Oluwaseun Olumide Okundalaye
Writing–review & editing: Necati Ozdemir, Mario Raso

Availability of data

The dataset used in this study, ALL_IDB (acute lymphoblastic leukemia image database), is publicly available and can be accessed online at https://www.kaggle.com/. No proprietary or restricted data were used.

AI tools statement

The authors used ChatGPT (OpenAI) to refine the language and organization of the manuscript. All research design, data analysis, and interpretation were performed independently by the authors. The authors accept full responsibility for the final content.

References

1. Bhargavav M. Acute lymphoblastic leukemia. In: *Hematologic Malignancies: Case Studies in Cytogenetic and Molecular Genetics.* Singapore: Springer Singapore; 2021;151-193. https://doi.org/10.1007/978-981-33-4799-1
2. Genovese A, Hosseini MS, Piuri V, Plataniotis KN, Scotti F. Acute lymphoblastic leukemia detection based on adaptive unsharpening and deep learning. In: *ICASSP 2021-2021 IEEE International Conference on Acoustics, Speech and Signal Processing (ICASSP).* New York: IEEE; 2021;1205-1209.https://doi.org/10.1109/ICASSP39728.2021.9414362
3. Malard F, Mohty M. Acute lymphoblastic leukaemia. *Lancet.* 2020;395:(10230):1146-1162. https://doi.org/10.1016/S0140-6736(19)33018-1
4. Leong SP, Witte MH. Lymphangiogenesis: Lymphatic system and lymph nodes; cancer lymphangiogenesis and metastasis. In: *Cancer Metastasis Through the Lymphovascular System.* New York: Springer; 2022:209-229. https://doi.org/10.1007/978-3-030-93084-4_21
5. Genovese A, Hosseini MS, Piuri V, Plataniotis KN, Scotti F. Histopathological transfer learning for acute lymphoblastic leukemia detection. In: *2021 IEEE International Conference on Computational Intelligence and Virtual Environments for Measurement Systems and Applications (CIVEMSA).* New York: IEEE. 2021:1-6. doi: 10.1109/CIVEMSA52099.2021.9493677
6. Jenkins, E. The biology of leukemia: the cancer of the blood. *Microrev Cell Mol Biol.* 2022; *9*).
7. Okikiolu J, Dillon R, Raj K. Acute leukaemia. *Medicine.* 2021;49(5):274-281. doi.org/10.1016/j.mpmed.2021.02.004
8. Chiorazzi N, Chen SS, Rai KR. Chronic lymphocytic leukemia. *Cold Spring Harb Perspect Med.* 2021;11(2):a035220. https://doi.org/10.1101/cshperspect.a035220
9. Osman AE, Deininger MW. Chronic myeloid leukemia: modern therapies, current challenges and future directions. *Blood Rev.* 2021;49:100825. https://doi.org/10.1016/j.blre.2021.100825
10. Stacy NI, Harvey JW. Structure of the bone marrow. In: *Schalm's Veterinary Hematology.* Hoboken, NJ: Wiley-Blackwell; 2022;18-26. https://doi.org/10.1002/9781119500537.ch3
11. Li R, Ma J, Chan Y, Yang Q, Zhang C. Symptom clusters and influencing factors in children with acute leukemia during chemotherapy. *Cancer Nurs.* 2022;43(5):411-418. https://doi.org/10.1097/NCC.0000000000000716
12. Hao TK, Hiep PN, Hoa NT, Ha CV. Causes of death in childhood acute lymphoblastic leukemia at Hue Central Hospital for 10 years (2008–2018). *Glob Pediatr Health.* 2020;7:2333794X20901930. https://doi.org/10.1177/2333794X20901930
13. Varghese N. Machine learning techniques for the classification of blood cells and the prediction of diseases. *Int J Comput Sci Eng.* 2020;9(1):66-75.
14. Khalil AJ, Abu-Naser SS. Diagnosis of blood cells using deep learning. *Int. J. Acad. Eng. Res.* 2022;6(2):69-84.
15. Vélez-Rodríguez I, Carranza-Aranda V. Damage mechanism of CK2 and IKAROS in Philadelphia-like acute lymphoblastic leukemia. *J Biosci Med.* 2024;12(4):49-59. https://doi.org/10.4236/jbm.2024.124005
16. Shiraz P, Jehangir W, Agrawal V. T-cell acute lymphoblastic leukemia—current concepts in molecular biology and management. *Biomedicines.* 2021;9(11):1621. https://doi.org/10.3390/biomedicines9111621
17. Khan S, Sajjad M, Hussain T, Ullah A, Imran AS. A review on traditional machine learning and deep learning models for WBCs classification in blood smear images. *IEEE Access.* 2020;9:10657-10673. https://doi.org/10.1109/ACCESS.2020.3048172

18. Yeasmin MN, Amin M, Joti TJ, Aung Z, Azim MA. Advances of AI in image-based computer-aided diagnosis: a review. *Array.* 2024;3:100357. https://doi.org/10.1016/j.array.2024.100357
19. Kumar A, Tyagi V, Singh H, Jain S. Advancing medical diagnostics on computer-assisted analysis for digital medicinal imagery. In: *Computer-Assisted Analysis for Digital Medicinal Imagery.* Hershey, PA: IGI Global; 2025:393-408. https://doi.org/10.4018/979-8-3693-5226-7.ch015
20. Zangana HM, Mohammed AK, Mustafa FM. Advancements and applications of convolutional neural networks in image analysis: a comprehensive review. *J Ilm Comput Sci.* 2024;3(1):16-29. https://doi.org/10.58602/jics.v3i1.30
21. Aydın S, Altun K. Early prediction of fabric quality using machine learning to reduce rework in manufacturing processes. *Int. J. Optimiz. Contro.* 2024;14(4):308-321. https://doi.org/10.11121/ijocta.1462
22. Ghazi FF, Tawfiq LN. Design optimal neural network based on new LM training algorithm for solving 3D-PDEs. *Int J Optimiz Contro.* 2024;14(3):249-260. https://doi.org/10.11121/ijocta.1519
23. Paswan S, Rathore YK. Detection and classification of blood cancer from microscopic cell images using SVM KNN and NN classifier. *Int J Adv Res Ideas Innov Technol.* 2017;3:315-324.
24. Calgan H. Optimal C-type filter design for wireless power transfer system by using support vector machines. *Int J Optimiz Contro.* 2023;13(2):151-160. https://doi.org/10.11121/ijocta.2023.1354
25. Abd Halim NH, Mashor MY, Hassan R. Classification of acute leukemia based on multilayer perceptron. *J Phys Conf Ser.* 2019;1372(1). https://doi.org/10.1088/1742-6596/1372/1/012044
26. Dasariraju S, Huo M, McCalla S. Detection and classification of immature leukocytes for diagnosis of acute myeloid leukemia using random forest algorithm. *Bioengineering.* 2020;7(4):120. https://doi.org/10.3390/bioengineering7040120
27. Prakisya NP, Liantoni F, Hatta P, Aristyagama YH, Setiawan A. Utilization of K-nearest neighbor algorithm for classification of white blood cells in AML M4, M5, and M7. *Open Eng.* 2021;11(1):662-668. https://doi.org/10.1515/eng-2021-0065
28. Jafarpisheh N, Zaferani EJ, Teshnehlab M, Karimipour H, Parizi RM, Srivastava G. A deep neural network combined with radial basis function for abnormality classification. *Mobile Netw Appl.* 2021;26(6):2318-2328. https://doi.org/10.1007/s11036-021-01835-0
29. Rismayanti N, Naswin A, Zaky U, Zakariyah M, Purnamasari DA. Evaluating thresholding-based segmentation and humoment feature extraction in acute lymphoblastic leukemia classification using Gaussian naïve Bayes. *Int J Artif Intell Med Issues.* 2023;1(2):74-83. https://doi.org/10.56705/ijaimi.v1i2.99
30. Yan T, Wong PK, Ren H, Wang H, Wang J, Li Y. Automatic distinction between COVID-19 and common pneumonia using multi-scale convolutional neural network on chest CT scans. *Chaos Solitons Fractals.* 2020;140:110153. https://doi.org/10.1016/j.chaos.2020.110153
31. Kumar A, Kumar M, Goswami P. Numerical solution of coupled system of Emden-Fowler equations using artificial neural network technique. *Int J Optimiz Contro.* 2024;14(1):62-73.
32. Liu Y, Pu H, Sun, DW. Efficient extraction of deep image features using convolutional neural network (CNN) for applications in detecting and analysing complex food matrices. *Trends Food Sci Technol.* 2021;113:193-204. https://doi.org/10.1016/j.tifs.2021.04.042
33. Hussain E, Hasan M, Rahman MA, Lee I, Tamanna T, Parvez MZ. CoroDet: a deep learning-based classification for COVID-19 detection using chest X-ray images. *Chaos Solitons Fractals.* 2021;142:110495. https://doi.org/10.1016/j.chaos.2020.110495
34. Sipes R, Li D. Using convolutional neural networks for automated fine-grained image 753848415classification753848415CECE753848415120563403 8AU: Please verify the updated publisher location in ref. (34). of acute lymphoblastic leukemia. In: *2018 3rd International Conference on Computational Intelligence and Applications (ICCIA).* New York: IEEE; 2018:157-161. https://doi.org/10.1109/ICCIA.2018.00036
35. Shafique S, Tehsin S. Acute lymphoblastic leukemia detection and classification of its subtypes using pretrained deep convolutional neural networks. *Technol Cancer Res Treat.* 2018;17:1533033818802789. https://doi.org/10.1177/1533033818802789
36. Pansombut T, Wikaisuksakul S, Khongkraphan K, Phon-On A. Convolutional neural networks for recognition of lymphoblast cell images. *Comput Intell Neurosci.* 2019;(1):7519603. https://doi.org/10.1155/2019/7519603
37. de Oliveira JEM, Dantas DO. Classification of normal versus leukemic cells with data augmentation and convolutional neural networks. In: *Proceeding of the VISIGRAPP.* Setúbal, Portugal: SciTePress; 4:685-692. https://doi.org/10.5220/0010257406850692
38. Zolfaghari M, Sajedi H. A survey on automated detection and classification of acute leukemia and WBCs in microscopic blood cells. *Multimed Tools Appl.* 2020;81:6723-6753. https://doi.org/10.1007/s11042-022-12108-7

39. Huang Y, Zhang J, Liu R, Zhao S. Improving accuracy and interpretability of CNN-based fault diagnosis through an attention mechanism. *Processes*. 2023;11(11):3233. https://doi.org/10.3390/pr11113233
40. Kadhim KA, Najjar FH, Waad AA, Al-Kharsan IH, Khudhair ZN, Salim AA. Leukemia classification using a convolutional neural network of AML images. *Mal J Fund Appl Sci*. 2023;19(3):306-312. https://doi.org/10.11113/mjfas.v19n3.2901
41. Kanavati F, Ichihara S, Tsuneki M. A deep learning model for breast ductal carcinoma in situ classification in whole slide images. *Virchows Arch.,* 2022;480(5):1009-1022. https://doi.org/10.1007/s00428-021-03241-z
42. Mustaqim T, Fatichah C, Suciati N. Deep learning for the detection of acute lymphoblastic leukemia subtypes on microscopic images: a systematic literature review. *IEEE Access*. 2023;11:16108-16127. https://doi.org/10.1109/ACCESS.2023.3245128
43. Genovese A, Piuri V, Scotti F. A decision support system for acute lymphoblastic leukemia detection based on explainable artificial intelligence. *Image Vis Comput*. 2024;151:105298. https://doi.org/10.1016/j.imavis.2024.105298
44. Archana R, Jeevaraj PE. Deep learning models for digital image processing: A review. *Artif Intell Rev*. 2024;57:11. https://doi.org/10.1007/s10462-023-10631-z
45. Talukder MA, Layek MA, Kazi M, Uddin MA, Aryal S. Empowering COVID-19 detection: optimizing performance through fine-tuned efficientnet deep learning architecture. *Comput Biol Med*. 2024;168:107789. https://doi.org/10.1016/j.compbiomed.2023.107789
46. Genovese A. ALLNet: acute lymphoblastic leukemia detection using lightweight convolutional networks. In: *2022 IEEE 9th International Conference on Computational Intelligence and Virtual Environments for Measurement Systems and Applications (CIVEMSA),* New York; 2022:1-6. https://doi.org/10.1109/CIVEMSA53371.2022.9853691
47. Kochhar A, Kaur P. Leveraging transfer learning for acute lymphoblastic leukemia cell classification: a deep learning approach. In: *International Conference on Innovative Computing and Communication*. Singapore: Springer Nature Singapore; 2025:187-200. https://doi.org/10.1007/978-981-96-7137-3_14
48. Muduli D, Parija S, Kumari S, Hassan A, Jangwan HS, Zamani AT, et al. Deep learning-based detection and classification of acute lymphoblastic leukemia with explainable AI techniques. *Array*. 2025;26. https://doi.org/10.1016/j.array.2025.100397
49. El Houby EM. Acute lymphoblastic leukemia diagnosis using machine learning techniques based on selected features. *Sci Rep*. 2025;15(1):28056. https://doi.org/10.1038/s41598-025-12361-4
50. Harithanush S, Poojitha K, Shalini R, Vandana B, Nithya R. LeukemiaVisionNet-21 deep neural network for automated acute lymphoblastic leukemia (ALL) classification. In: *2025 3rd International Conference on Data Science and Information Systems (ICDSIS)*. New York: IEEE; 2025:1-7. https://doi.org/10.1109/ICDSIS65355.2025.11070368
51. Genovese A, Piuri V, Scotti F. ALL-IDB patches: whole slide imaging for acute lymphoblastic leukemia detection using deep learning. In: *2023 IEEE International Conference on Acoustics, Speech, and Signal Processing Workshops (ICASSPW)*, New York: IEEE; 2023:1-5. https://doi.org/10.1109/ICASSPW59220.2023.10193429
52. Okundalaye OO, Özdemir N, Evirgen F. Leveraging machine learning for early and accurate anaemia diagnosis: a comparative study of classification algorithms. In: *International Conference on Mathematical Modelling, Applied Analysis and Computation*. Cham: Springer Nature; 2025:42-52.
53. Okundalaye O, Ozdemir N, Rotimi B, Akanbi F. Climate-based predictive modeling of malaria incidence using statistical and machine learning approaches. *Trans Comput Model Intell Syst*. 2025;1:10014. https://doi.org/10.65112/tcmis.10014
54. Sher M, Shah K, Ali Z, Abdeljawad T, Alqudah M. Using deep neural network in computational analysis of coupled systems of fractional integro-differential equations. *J Comput Appl Math*. 2025;474:116912. https://doi.org/10.1016/j.cam.2025.116912
55. Emin B, Alaca Y, Akmeşe ÖF, Karaca Y, Akgül A. Pixel map-based hybrid ai framework for early and accurate cardiovascular disease diagnosis. *J Comput Appl Math*. 2026;476:117095. https://doi.org/10.1016/j.cam.2025.117095
56. Hamou AA, Rasul RR, Hammouch Z, Özdemir N. Analysis and dynamics of a mathematical model to predict unreported cases of COVID-19 epidemic in Morocco. *Comp Appl Math*. 2022;41:289. https://doi.org/10.1007/s40314-022-01990-4
57. Genovese A, Piuri V, Plataniotis KN, Scotti F. DL4ALL: multi-task cross-dataset transfer learning for acute lymphoblastic leukemia detection. *IEEE Access*. 2023;11:65222-65237. https://doi.org/10.1109/ACCESS.2023.3289219
58. Okundalaye OO, Özdemir N, Awonusika RO. Early breast cancer prediction using optimized machine learning and tumor-immune modeling. *J Comput Appl Math*. 2026;473:116875.

https://doi.org/10.1016/j.cam.2025.116875
59. Olumide OO. Fractional-order gradient descent for enhancing deep learning optimization. *Asian Res J Math.* 2025;21(8):40-50. https://doi.org/10.9734/arjom/2025/v21i8970
60. Putzu L, Caocci G, Di Ruberto C. Leucocyte classification for leukaemia detection using image processing techniques. *Artif Intell Med.* 2014;62(3):179-191. https://doi.org/10.1016/j.artmed.2014.09.002
61. Joshi MD, Karode AH, Suralkar S. White blood cells segmentation and classification to detect acute leukemia. *Int J Emerg Trends Technol Comput Sci.* 2013;2(3):147-151.
62. Chatap N, Shibu S. Analysis of blood samples for counting leukemia cells using support vector machine and nearest neighbour. *IOSR J Comput Eng.* 2014;16(5):79-87. https://doi.org/10.9790/0661-16537987
63. MoradiAmin M, Samadzadehaghdam N, Kermani S, Talebi A. Enhanced recognition of acute lymphoblastic leukemia cells in microscopic images based on feature reduction using principle component analysis. *ront Biomed Technol.* 2015;2(3):128-136.
64. Rawat J, Singh A, Bhadauria HS, Virmani J, Devgun JS. Classification of acute lymphoblastic leukaemia using hybrid hierarchical classifiers. *Multimed Tools Appl.* 2017;76(18):19057-19085. https://doi.org/10.1007/s11042-017-4478-3

Okundalaye Oluwaseun Olumide *is a lecturer I in the Department of Mathematical Sciences, Adekunle Ajasin University, Akungba-Akoko, Nigeria. He holds a Ph.D. in Applied Mathematics from the University of Malaya, where he developed optimal homotopy asymptotic methods for nonlinear fractional models. His research focuses on optimization, numerical analysis, fractional differential equations, computational modeling, and machine-learning applications in health and science. Dr. Okundalaye has published widely in reputable journals, including IEEE Access and Journal of Computational and Applied Mathematics, with contributions spanning infectious-disease modeling, biomedical image analysis, and intelligent diagnostic systems. He teaches courses such as Optimization Theory, Numerical Analysis, and Mathematical Modeling, and has supervised numerous undergraduate and postgraduate projects. A recipient of the TETFund Ph.D. Scholarship and Ondo State Scholarship Award, he is committed to interdisciplinary research and the development of advanced mathematical and computational tools for solving real-world problems.*
https://orcid.org/0000-0003-1849-9690

Necati Özdemir *is a full professor and Head of the Department of Mathematics at Balıkesir University and also served as the Director of the Institute of Science. He earned his B.Sc. from Marmara University (1992), M.Sc. from the University of Warwick (1997), and Ph.D. from the University of Exeter (2000). Since joining Balıkesir University in 2000, he has held various academic and leadership roles, and Co-chair of international conferences, such as ICAME series. His research focuses on control theory, optimization, fractional calculus, financial mathematics, biological modeling, and numerical methods. Prof. Özdemir has published widely, serves on editorial boards of international journals, and is recognized among the top 3% of scientists in Turkey and globally by the AD Scientific Index. With a strong academic impact, he continues to advance applied mathematics and mentor future scholars.*
https://orcid.org/0000-0002-6339-1868

Akinsunmade Akintayo Emmanuel *is a lecturer in the Department of Mathematics at the University of Medical Sciences, Ondo, Nigeria. He holds a Ph.D. in Mathematics with a specialization in Optimization, reflecting his strong interest in solving complex real-world problems through advanced mathematical modeling and analytical methods. His research spans optimization techniques, applied mathematics, and the development of efficient computational approaches to support decision-making in science, health, and engineering. Dr. Akinsunmade has published scholarly articles in reputable journals and actively contributes to the advancement of mathematics education and research in Nigeria. In addition to his research, he is committed to teaching and mentoring, inspiring the next generation of mathematicians and scientists to apply mathematical knowledge to practical challenges. With a passion for academic excellence and innovation, Dr. Emmanuel continues to engage in collaborative projects that foster interdisciplinary research and contribute to global knowledge development.*
https://orcid.org/0000-0001-5285-0267

Oluwaseun Onuoha *is a lecturer in the Department of Mathematics at Adekunle Ajasin University, Ondo, Nigeria. She earned her Ph.D. in Applied Mathematics from the University of Ilorin, where she specialized in advanced mathematical methods and their practical applications. Her research spans optimization, applied mathematics, and mathematical modeling, with a focus on creating innovative solutions to pressing scientific and societal challenges. She has published in peer-reviewed journals and actively collaborates with researchers both within*

Nigeria and internationally. Passionate about the power of mathematics to drive education, technology, and development, she is committed to helping students think critically and apply mathematical tools to solve real-world problems across different fields.
https://orcid.org/0000-0001-9135-1217

Mario Raso *received a master's degree in Computer Engineering and a Ph.D. in Computer Science from Sapienza University of Rome, Italy. His research focuses on cryptography and cybersecurity, with particular attention to the design and analysis of secure protocols. He has contributed to several international research projects and published in leading peer-reviewed journals and conference proceedings in the field of information security. His work spans both the theoretical foundations of cryptographic primitives and their practical applications to real-world security challenges. His long-term goal is to advance the state of secure and trustworthy computing systems to address emerging digital threats.*
https://orcid.org/0000-0001-9495-3037

An International Journal of Optimization and Control: Theories & Applications
(https://accscience.com/journal/ijocta)